Tuned Three-Level Flying Capacitor Power Amplifier for Visible Light Communication

Juan R. Garcia-Mere
Electronic Power Supply Systems Group (SEA), University of Oviedo
Gijon, Spain
garciamjuan@uniovi.es

Juan Rodriguez
Electronic Power Supply Systems Group (SEA), University of Oviedo
Gijon, Spain
rodriguezmjuan@uniovi.es

Diego G. Lamar
Electronic Power Supply Systems Group (SEA), University of Oviedo
Gijon, Spain
gonzalezdiego@uniovi.es

Javier Sebastian
Electronic Power Supply Systems Group (SEA), University of Oviedo
Gijon, Spain
sebas@uniovi.es

***Abstract*—Visible Light Communication (VLC) is a wireless communication technology that uses visible light to send data. The most popular implementation of a VLC driver is made up of a DC-DC converter, in charge of biasing a set of High-Brightness LEDs (HB-LEDs), and a Linear Power Amplifier (LPA), that injects the communication signal component. In this work, a Switching-Mode Power Amplifier (SMPA) based on a tuned three-level Flying Capacitor (FC) topology is proposed as an alternative to overcome the poor power efficiency of the aforementioned LPAs. In comparison to other SMPA topologies, the proposed SMPA is able to reproduce Single-Carrier Modulation (SCM) schemes with a higher bandwidth due to the proposed phase-shift control strategy and the use of a multilevel approach. A prototype reproducing a SCM scheme was tested, achieving a peak power efficiency of 96% and improving the efficiency results of other existing SMPAs approaches that were previously proposed for this kind of applications.**

Keywords—Visible Light Communication (VLC), Flying Capacitor (FC), Switching-Mode Power Amplifiers (SMPAs), Quadrature Amplitude Modulation (QAM).

I. Introduction

Visible Light Communication (VLC) has been explored during recent years as an alternative communication technology to alleviate the saturation of the radiofrequency (RF) spectrum [1]-[3]. VLC uses the visible light part of the electromagnetic spectrum (430 THz-750 THz) to transmit information in a non-guided medium instead of RF waves. One of the main advantages of VLC over the use of RF communication is the low cost and the low complexity required by the deployment of the networks that make use of this technology, since it can be integrated into the current Solid-State Lighting (SSL) architectures. Thus, VLC achieves the combination of the transmission of information with the illumination functionality.

In a VLC link, the communication is performed modulating the current that flows through a set of High Brightness LEDs (HB-LEDs) which translates the fast current changes into proportional light intensity variations. The synthesis of the current that flows through these HB-LEDs can be splitted into two main components. First, a positive DC bias is required to comply with the illumination functionality, and it will determine the lighting level. Second, the information to be transmitted will be encoded into AC variations around the operating point, according to the reproduced modulation scheme. In order to optimize the electrical bandwidth of the HB-LEDs used in the existing SSL luminaires, the frequency of the current variations corresponding to the communication signal should be of few MHz. Note that the conventional white HB-LEDs used in the commercial SSL luminaires have a bandwidth between 3 and 5 MHz [4].

The design of the circuitry that drives the HB-LEDs of a VLC transmitter (i.e., the VLC driver) has been subject of discussion during the last years [5], [6]. Although many high efficiency HB-LED drivers mainly focused on illumination tasks are reported in the literature [7], it should be considered that the inclusion of transmission capabilities in a VLC driver always results in additional power losses [8].

One of the most popular VLC driver implementations is the bias-T architecture, depicted in Fig. 1 [5]. In this architecture, the aforementioned current variations are performed by changing the voltage applied to the string of HB-LEDs (v_o). The current that determines the illumination level is synthesized by means of a high-efficiency DC-DC converter, which generates a DC voltage level (V_{o-DC}) to bias the HB-LED string in its linear region. At the same time, a Linear Power Amplifier (LPA) synthesizes voltage variations (v_{o-AC}) according to the communication signal reference (v_{AC-ref}) to be transmitted. Both components are then combined using a choke inductor and a coupling capacitor, respectively.

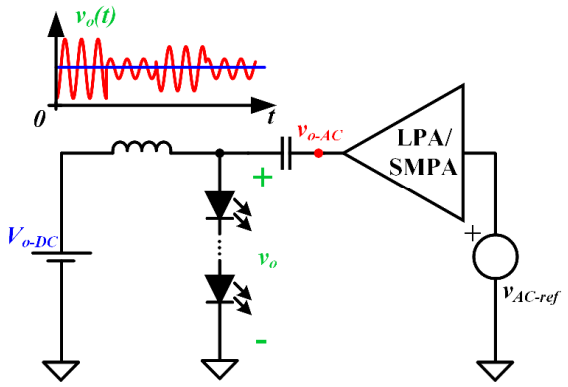

Fig. 1: The bias-T VLC driver architecture.

Although Class A and Class A/B LPAs provide high data transfers, the power efficiencies reported are very poor (10% - 40%) [9], [10]. In recent years, the use of Switching-Mode Power Amplifiers (SMPAs) has been proposed as an alternative to the conventional LPAs used in VLC transmitters. As an example, two Class E SMPAs are used in [11] to transmit a Single-Carrier Modulation (SCM) (i.e., the amplitude and the phase of the communication carrier depend on the information to be transmitted). Although the SMPA achieves an efficiency of 72%, the approach results in a very complex VLC driver. Furthermore, power devices able to withstand high voltage stresses are required to implement both amplifiers, and a bulky inductor is mandatory. In addition, Zero Voltage Switching (ZVS) is lost always when a change in the carrier occurs, with a ZVS recovery period of nearly two carrier cycles. In this way, one of the main advantages of Class E SMPA is lost. Another approach consists in using fast switched-mode DC-DC converters to provide not only the biasing component, but also the communication signal [12]-[15]. However, the bit rates achieved with these approaches are not as high as those achieved with the aforementioned LPAs. Moreover, it leads to bulky solutions when SCM schemes are reproduced (for instance, two DC-DC converters, one of them implementing a 6th order output filter, are used in [15]).

In this work, a SMPA based on a tuned three-level Flying Capacitor (FC) topology is proposed to be used in a bias1T architecture for implementing a VLC driver. This topology reduces the switching losses in comparison to other SMPAs used for communication signal synthesis, which are critical due to the high bandwidth required. In addition, the use of a multilevel topology with the proposed phase-shift control strategy provides the enhancement of different aspects in comparison to other SMPA approaches, in particular the bandwidth of the communication signal to be reproduced. The rest of this article is organized as follows. In Section II, the SMPA based on the FC topology is presented, and an analysis of its operating principle along with the proposed phase-shift strategy control is provided. In Section III, an analysis of the dynamic improvements of the SMPA against a conventional Class D SMPA is introduced. In Section IV, the operation of the SMPA is experimentally tested using a prototype capable of reproducing SCM schemes with a carrier of 1 MHz. Finally, the main conclusions of this work are given in Section V.

II. Tuned SMPA based on the FC Topology

A. Requirements for the Communication Signal Synthesis

One of the most used SCM schemes, and whose reproduction is the object of this work, is the Quadrature Amplitude Modulation (QAM) scheme. One of the reasons to use this kind of modulations is the high spectral efficiency they provide [16], [17]. In these schemes, a sinusoidal signal of frequency f_0 varies both its amplitude and phase according to the digital symbol (i.e., a certain set of bits) to be transmitted. Thus, if a sequence of QAM symbols is used for data transfer, the waveform to be synthesized by the power amplifier of the VLC driver in a bias-T architecture during the transmission of the k^{th} symbol, can be expressed as

$$s_k(t) = A_k \cos(2\pi f_0 t + \phi_k), \quad (1)$$

where A_k and ϕ_k are the amplitude and the phase of the carrier corresponding to the encoding of the k^{th} symbol according to the QAM scheme used, respectively.

B. Operating Principle

In order to synthesize the aforementioned QAM scheme, this work proposes the use of SMPAs based on the use of the FC topology [18]-[20]. This kind of circuits has raised interest in the synthesis of signals using Pulse-Width Modulation (PWM) techniques [21], [22]. Some of the advantages that this topology offers this topology are the possibility of implementing a multilevel architecture without the need of auxiliary input voltage sources, the reduction of the harmonic content at the output voltage and the reduction of the switching losses. In addition, a method for reproducing passband signals using a multilevel pulse train is proposed in [23] as an alternative to the high switching losses of the conventional PWM techniques. This idea is adapted in this work to implement a multilevel SMPA based on the FC topology (hereafter, three-level Class D SMPA), shown in Fig. 2.

It should be noted that the resistive load R_{LED} included in Fig. 2 models the dynamic resistance of a set of HB-LEDs already biased by a regular DC-DC converter in the bias-T architecture. For the sake of simplicity, this DC-DC converter has not been represented in this schematic.

The proposed SMPA is made up of two pairs of MOSFETs (S_{A1}, S_{B1}) and (S_{A2}, S_{B2}), which are controlled complementarily, following the phase-shift control strategy shown in Fig. 3 and Fig. 4. The switching frequency of the MOSFETs is equal to the carrier frequency f_0, and they are ON half the switching period. Following this control strategy, the AC component of the voltage at the input of the filter (v_{sw}) is made up of the difference between two pulses with a phase difference of 180° (i.e., the relative positions of the two pulses within the switching period is γ and $\gamma + 1/2$), with the same duty cycle (d) and with the same amplitude (i.e., $V_g/2$, where V_g is the supply voltage of the proposed SMPA). The width of both pulses can be varied by means of d parameter (phase-shift between control pulses of S_{A1} and S_{A2}), and its position by means of parameter γ. v_{sw} is then filtered using the LC band-pass filter made up of the inductance L_0 and capacitor C_0 (see Fig. 2). This filter is tuned to the frequency f_0. Therefore, the SMPA output signal v_{o-AC} applied to the string of HB-LEDs could be simplified as the first switching harmonic of v_{sw}. It should be considered that the capacitor C_0 of the band-pass filter acts, at the same time, as the coupling capacitor of the bias-T architecture shown in Fig. 1, thus reducing the number of components required to implement a fully functional VLC driver.

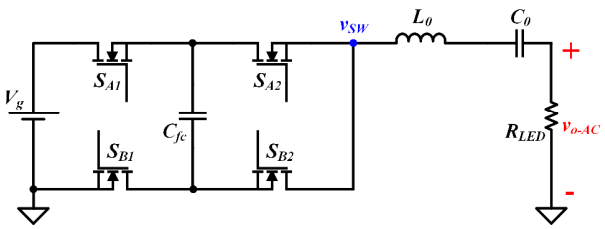

Fig. 2: Proposed three-level FC Class D SMPA.

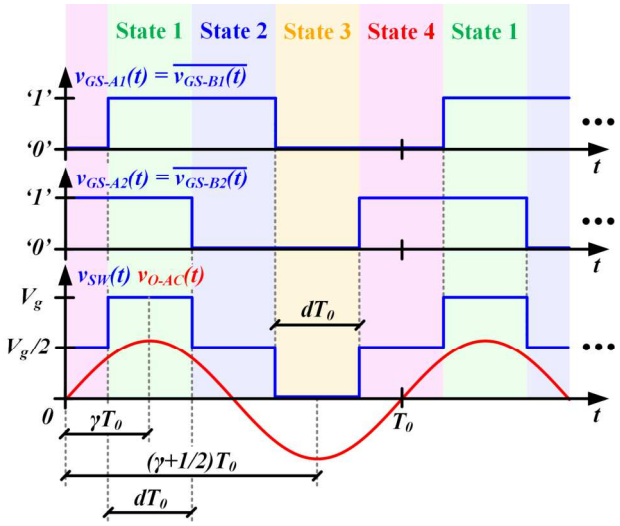

Fig. 3: Driving signals and main waveforms of the proposed three-level FC Class D SMPA operating under the phase-shift control strategy.

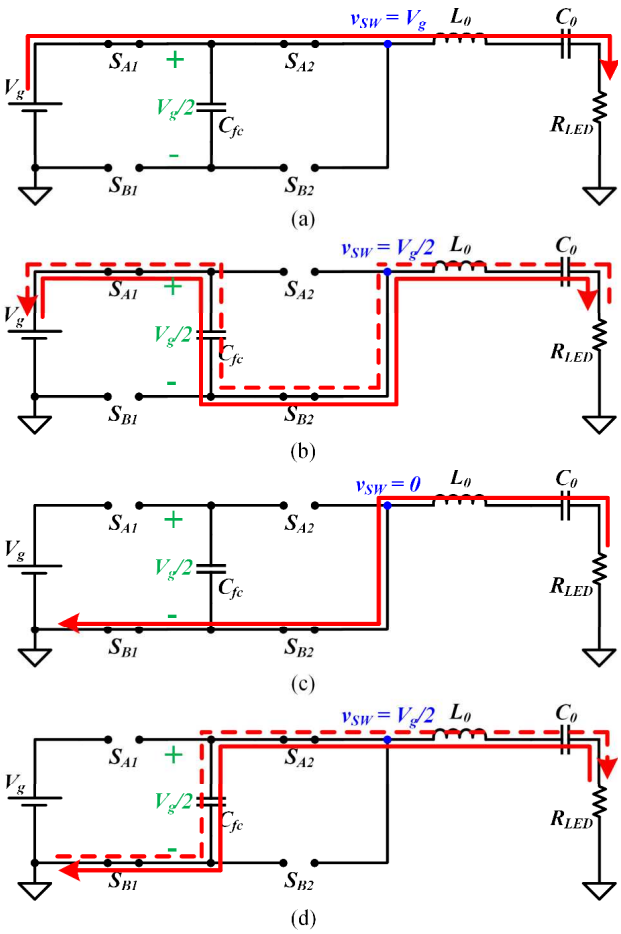

Fig. 4: Equivalent circuits of the proposed three-level FC Class D SMPA: (a) State 1. (b) State 2. (c) State 3. (d) State 4.

Another possible option for implementing a three-level SMPA may involve the use of a full bridge [24]. However, as the switching signal is not referenced to ground, a transformer would be needed to use in the bias-T architecture of Fig. 1, thus increasing the size of the VLC driver to be integrated in the HB-LED luminaire.

C. Synthesis of QAM schemes

To understand how the proposed three-level FC Class D SMPA can be used to synthesize QAM schemes, the theoretical expression of the signal obtained at the output of the circuit has to be derived. The signal v_{sw} can be expressed as a function of its harmonics by using the Fourier analysis

$$v_{sw}(t) = \frac{V_g}{2} + \frac{2}{\pi} V_g \sum_{n=1}^{\infty} \frac{\sin[(2n-1)\pi d]}{2n-1} \cdot \cos[(2n-1)\omega_0 t - (2n-1)2\pi\gamma], \quad (2)$$

where $\omega_0 = 2\pi f_0$. It has to be considered that parameter d varies from 0 to 0.5 (i.e., both switching pulses never overlap), while parameter γ varies from 0 to 1. Assuming that the series LC output filter in Fig. 2 is tuned at f_0, the rest of frequency components of the signal v_{sw} ($n \neq 1$) are attenuated, and therefore can be considered theoretically rejected at the output of the circuit. Thus, the output voltage waveform v_{o-AC} of the proposed SMPA can be expressed as

$$v_{o\text{-}AC}(t) = \frac{2}{\pi} V_g \sin(\pi d) \cos(\omega_0 t - 2\pi\gamma). \quad (3)$$

As equation (3) shows, amplitude and phase changes of the sinusoidal waveform obtained at the output of the SMPA can be carried out by changing d and γ, respectively. In this way, the transmission of a QAM scheme can be achieved adjusting both control parameters according to the amplitude and the phase of the digital symbol to be transmitted.

D. Circuit States

Fig. 4 depicts the four circuit modes that appear during the operation of the three-level FC Class D SMPA under the proposed phase-shift control strategy, including the main current paths. For the sake of simplicity, it is considered that the voltage across the floating capacitor C_{fc} (see Fig. 2) is constant and equal to $V_g/2$. Hence, the description of each state during a switching cycle can be found below:

- State 1 (S_{A1} = ON, S_{A2} = ON, Fig. 4(a)): during this state, v_{sw} is clamped to V_g and current flows from the input voltage source to the load. It is considered that the current through the load is a sinusoidal waveform due to the resonant output filter, and it is in phase with voltage due to the resistive behavior of the HB-LED load. As Fig. 3 depicts, operation in this state occurs during the positive half-cycle of the carrier.
- State 2 (S_{A1} = ON, S_{A2} = OFF, Fig. 4(b)): v_{sw} is equal to $V_g/2$, which is the difference between the voltage provided by the input voltage source (i.e., V_g) and the voltage across C_{fc} (i.e., $V_g/2$). Due to the sinusoidal behavior of the load current, a change in its direction occurs during the second half of the interval. This is represented in Fig. 4(b) with a dotted line. Thus, C_{fc} is first being charged from the supply source and then

discharged by the load current. Therefore, the average current during this time interval is zero.

- State 3 (S_{A1} = OFF, S_{A2} = OFF, Fig. 4(c)): this state occurs during the negative half-cycle of the sinusoidal load current. Therefore, current flows from the load to ground. v_{sw} is clamped to 0 V, and C_{fc} is disconnected.
- State 4 (S_{A1} = OFF, S_{A2} = ON, Fig. 4(d)): C_{fc} is connected to the input of LC band-pass filter. Thus, the switching node voltage during this interval is $V_g/2$. In this case, the same situation as the one of state 2 occurs: a change in the load current direction during the second half of the interval varies the C_{fc} charging process.

As explained, the phase-shift control strategy previously described makes the average current through C_{fc} equal to zero under the nominal operation of the SMPA. Thus, the use of a tuned FC topology reproducing a sinusoidal current achieves a natural mechanism to balance the charge of C_{fc}, ensuring that the voltage across the flying capacitor remains constant. This self-balancing mechanism reduces the complexity in the implementation of the FC topology in comparison to other approaches under PWM operation, where an active control is required to keep the voltage across C_{fc} constant [22], [25], [26].

III. Improvement of the Communication Signal Bandwidth

From the communication perspective, the three-level FC Class D SMPA improves different aspects of the synthesis of a QAM scheme, in comparison with other conventional SMPA approaches, like the tuned Class D SMPA (see Fig. 5), which is the two-level version of the topology proposed in this paper. In the Class D SMPA, MOSFETs S_A and S_B operate complementary, generating voltage pulses of frequency f_0 and amplitude V_g at the switching node. The pulse-width and the pulse-phase can be controlled with d and γ parameters, respectively. In this case, the analysis of v_{sw} leads to the following expression

$$v_{sw}(t) = dV_g + \frac{2}{\pi} V_g \sum_{n=1}^{\infty} \frac{\sin(n\pi d)}{n} \cos(n\omega_0 t - n2\pi\gamma). \quad (4)$$

Considering that the resonant circuit formed by L_0 and C_0 is tuned to f_0, the expression of the SMPA output signal v_{o-AC} is the same as the one shown in equation (3). As can be seen, an independent control of the amplitude and the phase of a carrier by means of the parameters d and γ, respectively, can be achieved. Thus, a tuned Class D SMPA can also be used to synthesize QAM schemes in the same way the three-level FC Class D SMPA does.

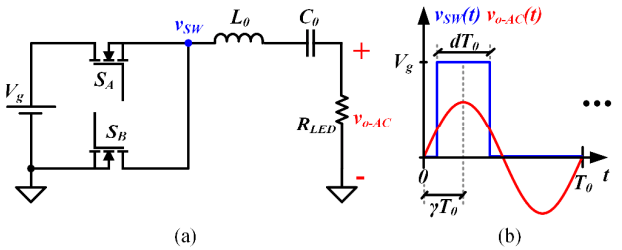

Fig. 3: Tuned Class D SMPA: (a) Topology. (b) Main voltage waveforms.

The main difference between the three-level and the two-level approaches lies in the rejection of the even harmonics that the phase-shift control achieves in the case of the SMPA topology introduced in this work. It has a direct effect on the bandwidth of the output band-pass filter and, therefore, on the communication bandwidth. In the case of the two-level approach, the upper cut-off frequency $f_{sup-2level}$ of the band-pass filter shall suffice the following condition in order to properly reproduce the communication signal without distortion

$$f_{max} < f_{upper\text{-}2level} < 2f_0 . \quad (5)$$

In the case of the proposed three-level SMPA, the upper cut-off frequency $f_{upper-3level}$ must satisfy the following requirement

$$f_{max} < f_{upper\text{-}3level} < 3f_0 . \quad (6)$$

In these expressions, f_{max} represents the maximum frequency of the communication signal, that, in the case of a QAM scheme, can be approximated as [16]

$$f_{max} = f_0 + f_{sym} = \left(1 + \frac{1}{m}\right) f_0 , \quad (7)$$

where f_{sym} is the symbol frequency (i.e., the frequency at which the digital symbols are sent), and m the number of carrier periods required by the transmission of a digital symbol. In the literature, the quality factor Q of a band-pass filter is used as a figure of merit to define the relationship between the tuning frequency f_0 and the bandwidth of the filter $\Delta f = f_{upper} - f_{lower}$ [27]:

$$Q = \frac{f_0}{\Delta f} . \quad (8)$$

Regarding the dynamics of a SMPA, the lower the Q value of the output band-pass filter, the higher the communication bandwidth, and therefore, the higher the data transfer rate. Nevertheless, the election of the value of parameter Q will also influence in the attenuation degree of the rest of v_{sw} switching harmonics, and therefore, in the distortion of the reproduced communication signal. Due to the phase-shift control strategy and the rejection of the even harmonics, it can be proven that the three-level SMPA approach offers a better tradeoff between the bandwidth and the distortion of the reproduced signal than a traditional two-level SMPA.

The average total harmonic distortion $\overline{\text{THD}}$ (where THD stands for Total Harmonic Distortion) is introduced in this paper as a figure of merit to compare the distortion introduced by different band-pass filters with different Q values when reproducing the whole range of possible carrier amplitudes. This figure of merit is defined as

$$\overline{\text{THD}}[\%] = \frac{100}{A_{max}} \int_0^{A_{max}} \text{THD}(A) dA, \quad (9)$$

where A_{max} is the maximum amplitude of the communication carrier that can be synthesized at the output of the SMPA, and

THD(A) the value of the total harmonic distortion when a carrier with amplitude A is reproduced. Note that the range of possible carrier amplitudes varies from 0 ($d = 0$ in both the two-level and three-level approaches) to A_{max} ($d = 0.5$). The value of THD(A) is defined as [28]

$$\mathrm{THD}(A) = \frac{\sqrt{\sum_{n=2}^{\infty} V_n^2}}{V_1^2}, \tag{10}$$

where V_n is the rms value of the n^{th} harmonic of the SMPA output voltage waveform, and V_1 the rms value of its fundamental component (i.e., the communication carrier). Fig. 6 shows the range of possible THD values in a carrier synthesis using both a two-level and a three-level SMPA applying equation (10).

The most suitable design of the output LC filter of a tuned SMPA will consist in finding the Q value that limits a maximum THD value. As an example, Fig. 7 shows the simulation results when the same amplitude change is performed in a communication carrier whose frequency is f_0 = 1 MHz, using a two-level and a three-level SMPA approach. The tuned Class D SMPA requires a value of $Q = 12$ to reach a THD of 5%, while in the three-level FC Class D SMPA, a Q value of 5 is enough to reach the same THD value. It is observed that the lower the Q value is, the faster the transition will be since the bandwidth of the output band-pass filter will be higher. It means that every digital symbol will require more carrier cycles for its transmission in a tuned Class D SMPA than in a three-level FC Class D SMPA, thus resulting in a slower data transfer. The value of the symbol frequency f_{sym} that can be reproduced with a certain value of Q can be approximated as [16], [17]

$$f_{sym} = \frac{f_0}{2Q}, \tag{11}$$

where the bandwidth required by the transmission of a QAM scheme is considered to be $2f_{sym}$. In Fig. 8, the positive half-spectra of the signal at the switching node when synthesizing a 16-QAM scheme with the two-level and three-level approaches are plotted, with the f_{sym} values imposed by the previously estimated Q values. The magnitude Bode diagrams of the output band-pass filters used in each SMPA are also represented. As Fig. 8 shows, the bandwidth of the communication signal reproduced by the three-level Class D SMPA is greater than in a conventional tuned Class D SMPA while keeping the same THD value, due to the reduction of Q.

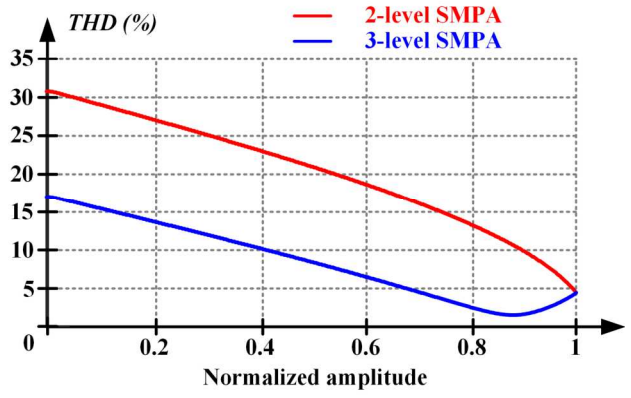

Fig. 6: THD value obtained when different carrier amplitudes are synthesized using a two-level SMPA and a three-level approach for the same output LC filter ($Q = 5$).

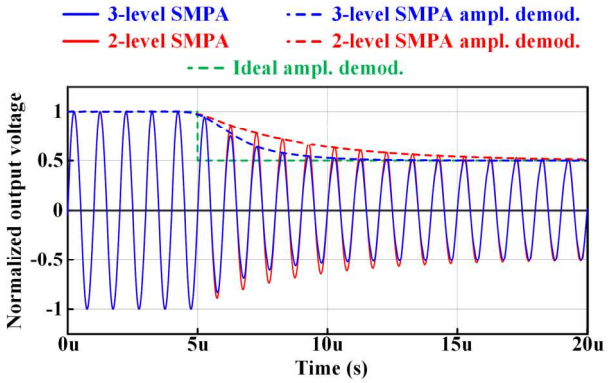

Fig. 7: Amplitude transition using a two-level SMPA and a three-level SMPA approach, considering THD = 5%.

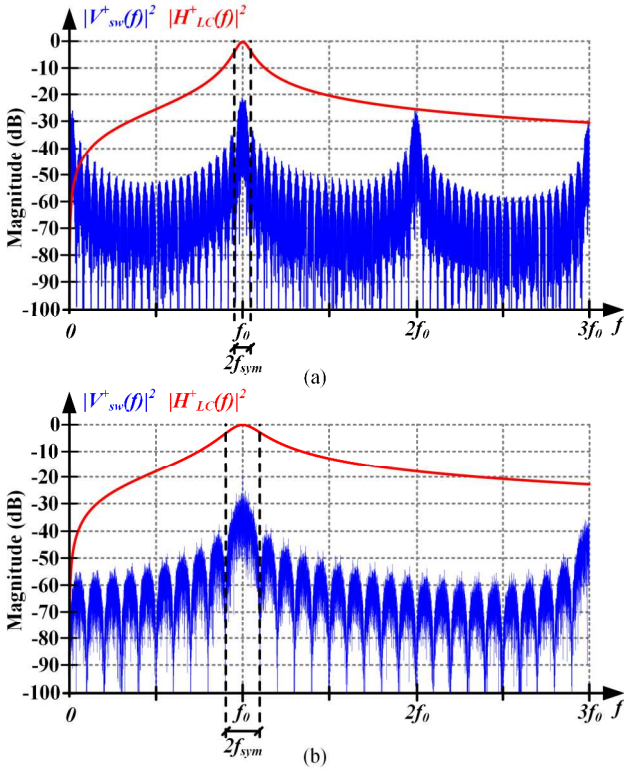

Fig. 8: Spectrum of v_{sw} and frequency response of the output band-pass filter: (a) Tuned Class D SMPA and $Q = 12$. (b) Three-level FC Class D SMPA and $Q = 5$.

IV. Experimental Results

In order to evaluate the operation of the proposed SMPA, a prototype that drives a load of 32 XLamp MX-3 HB-LEDs (arranged in 4 parallel strings of 8 HB-LEDs per string) has been implemented and tested. CSD17527Q5A MOSFETs are used to implement the switching cells. The frequency of the communication carrier is equal to 1 MHz. The *LC* band-pass filter design has led to a Q value of 3 (L_0 = 1.9 µH and C_0 = 13.26 nF). In order to verify the operation of the prototype, the reproduction of an unmodulated carrier (sinusoidal waveform with constant amplitude and phase) was evaluated (see Fig. 9). The figure depicts both the voltage waveform obtained at the switching node and the signal synthesized at the HB-LED load, as well as the current provided by the SMPA to the HB-LED arrangement. An external DC-DC power supply has been used to correctly bias the set of HB-LEDs in its linear zone (I_{o-DC} = 1 A). The supply voltage V_g of the prototype is set to 5 V. As can be seen, v_{sw} remains constant and equal to $V_g/2$ during the conduction states 2 and 4. Thus, the experimental results validate the self-balancing process of the flying capacitor C_{fc} voltage previously described. Fig. 10 shows the reproduction of a carrier when amplitude and phase changes are performed, thus representing the typical operation of a QAM transmitter. The power efficiency results of the prototype when reproducing carriers with different amplitudes is shown in Fig. 11. It can be seen that a peak efficiency of 96 % and an average efficiency of 85.72% are achieved, when the whole range of possible amplitudes are considered.

V. Conclusion

In this work, the design of a tuned three-level FC topology has been presented as a novel SMPA to be used in a bias-T VLC driver architecture. This topology is capable of synthesizing communication signals with a higher bandwidth than those reproduced by other SMPA approaches, due to the proposed phase-shift control strategy. For this purpose, a theoretical analysis of the improvements that this FC-based SMPA offers in comparison with the tuned Class D amplifier in the synthesis of QAM schemes has been performed. Furthermore, the phase1shift control strategy also allows for the implementation of a self-balancing mechanism that ensures that the voltage across the flying capacitor remains constant, unlike other FC implementations. The idea has been successfully evaluated through the implementation of a prototype capable of reproducing QAM schemes, with a peak power efficiency of 96%.

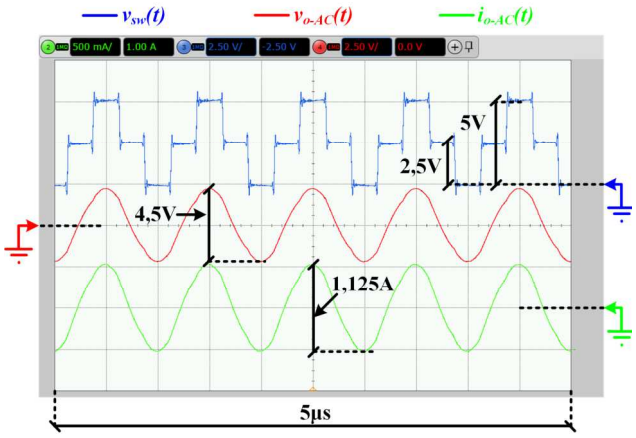

Fig. 9: Main waveforms when an unmodulated carrier is reproduced.

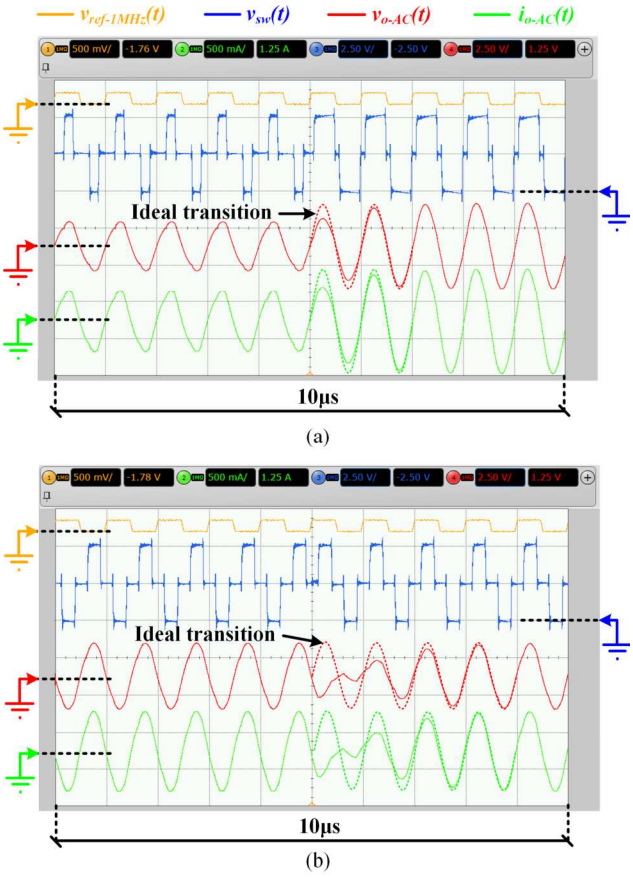

Fig. 10: Reproduction of changes in the communication carrier: (a) Amplitude change (b) Phase change.

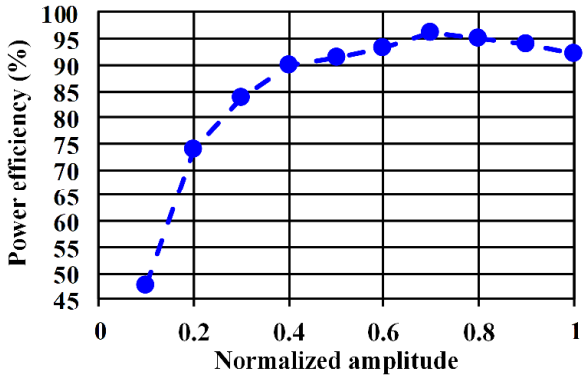

Fig. 11: Power efficiency of the prototype as a function of the amplitude of the carrier to be reproduced.

Acknowledgements

This work was supported in part by the Spanish Government under Project MCI-20-PID2019-110483RB-I00 and Project MCI-21-PDC2021-121242-I00 and in part by the Principality of Asturias under Project SV-PA-21-AYUD/2021/51931, by the FEDER funding and "Severo Ochoa" Program Grant no. BP20-181.

REFERENCES

[1] *Visible Light Communication (VLC)–A Potential Solution to the Global Wireless Spectrum Shortage*. London: GBI Res., September 2011.

[2] H. Elgala, R. Mesleh and H. Haas, "Indoor optical wireless communication: potential and state-of-the-art," in *IEEE Communications Magazine*, vol. 49, no. 9, pp. 56-62, September 2011.

[3] P. H. Pathak, X. Feng, P. Hu and P. Mohapatra, "Visible Light Communication, Networking, and Sensing: A Survey, Potential and Challenges," in *IEEE Communications Surveys & Tutorials*, vol. 17, no. 4, pp. 2047- 2077, Fourth Quarter 2015.

[4] A. J. Roufs and F. J. J. Blommaizt, "Temporal Impulse and Step Responses of the Human Eye Obtained Psychophysically by Means of a Drift-Correction Perturbation Technique," in *Vision Research*, vol. 21, no. 8, pp. 1203-21, 1981.

[5] L. Teixeira, F. Loose, J. M. Alonso, C. H. Barriquello, V. Alfonso Reguera and M. A. Dalla Costa, "A Review of Visible Light Communication LED Drivers," in *IEEE Journal of Emerging and Selected Topics in Power Electronics*, vol. 10, no. 1, pp. 919-933, Feb. 2022.

[6] J. Sebastian, D. G. Lamar, D. G. Aller, J. Rodríguez and P. F. Miaja, "On the Role of Power Electronics in Visible Light Communication," in *IEEE Journal of Emerging and Selected Topics in Power Electronics*, vol. 6, no. 3, pp. 1210-1223, Sept. 2018.

[7] Y. Wang, J. M. Alonso and X. Ruan, "A Review of LED Drivers and Related Technologies," in *IEEE Transactions on Industrial Electronics*, vol. 64, no. 7, pp. 5754-5765, July 2017.

[8] A. Tsiatmas, F. M. Willems, J. -P. M. Linnartz, S. Baggen and J. W. Bergmans, "Joint illumination and visible-Light Communication systems: Data rates and extra power consumption," in *2015 IEEE International Conference on Communication Workshop (ICCW)*, 2015.

[9] J. Vucic, C. Kottke, S. Nerreter, K. Langer and J. W. Walewski, "513 Mbit/s Visible Light Communications Link Based on DMT-Modulation of a White LED," in *Journal of Lightwave Technology*, vol. 28, no. 24, pp. 3512-3518, Dec.15, 2010.

[10] H. Li, X. Chen, J. Guo, Z. Gao and H. Chen, "An analog modulator for 460 MB/S visible light data transmission based on OOK-NRS modulation," in *IEEE Wireless Communications*, vol. 22, no. 2, pp. 68-73, April 2015.

[11] D. G. Aller, D. G. Lamar, P. F. Miaja, J. Rodríguez and J. Sebastián, "Taking Advantage of the Sum of the Light in Outphasing Technique for Visible Light Communication Transmitter," in *IEEE Journal of Emerging and Selected Topics in Power Electronics*, vol. 9, no. 1, pp. 138-145, Feb. 2021.

[12] V. M. de Albuquerque, G. M. Soares, J. M. Alonso and P. S. Almeida, "A Simple Resonant Switched-Capacitor LED Driver Employed as a Fast Pulse-Based Transmitter for VLC Applications," in *IEEE Journal of Emerging and Selected Topics in Power Electronics*, vol. 9, no. 1, pp. 111-122, Feb. 2021.

[13] F. Loose, L. Teixeira, R. R. Duarte, M. A. Dalla Costa and C. H. Barriquello, "On the Use of the Intrinsic Ripple of a Buck Converter for Visible Light Communication in LED Drivers," in *IEEE Journal of Emerging and Selected Topics in Power Electronics*, vol. 6, no. 3, pp. 1235-1245, Sept. 2018.

[14] J. Rodríguez Mendez, D. G. Lamar, D. G. Aller, P. F. Miaja and J. Sebastián, "Reproducing Multicarrier Modulation Schemes for Visible Light Communication With the Ripple Modulation Technique," in *IEEE Transactions on Industrial Electronics*, vol. 67, no. 2, pp. 1532-1543, Feb. 2020.

[15] J. Rodríguez, D. G. Lamar, P. F. Miaja, D. G. Aller and J. Sebastián, "Power-Efficient VLC Transmitter Based on Pulse-Width Modulated DC–DC Converters and the Split of the Power," in *IEEE Transactions on Power Electronics*, vol. 34, no. 2, pp. 1726-1743, Feb. 2019.

[16] E. McCune, *Practical digital wireless signals (The Cambridge RF and Microwave Engineering Series)*. Cambridge: Cambridge University Press, 2010.

[17] F. Xiong, *Digital Modulation Techniques*. Boston: Artech House Telecommunications Library, 2006.

[18] Jih-Sheng Lai and Fang Zheng Peng, "Multilevel converters-a new breed of power converters," in *IEEE Transactions on Industry Applications*, vol. 32, no. 3, pp. 509-517, May-June 1996.

[19] J. Rodriguez, Jih-Sheng Lai and Fang Zheng Peng, "Multilevel inverters: a survey of topologies, controls, and applications," in *IEEE Transactions on Industrial Electronics*, vol. 49, no. 4, pp. 724-738, August 2002.

[20] F. Canales, P. Barbosa and F. C. Lee, "A zero-voltage and zero-current switching three-level DC/DC converter," in *IEEE Transactions on Power Electronics*, vol. 17, no. 6, pp. 898-904, November 2002.

[21] Y. Lei et al., "A 2-kW Single-Phase Seven-Level Flying Capacitor Multilevel Inverter With an Active Energy Buffer," in *IEEE Transactions on Power Electronics*, vol. 32, no. 11, pp. 8570-8581, Nov. 2017.

[22] V. Yousefzadeh, E. Alarcon and D. Maksimovic, "Three-level buck converter for envelope tracking applications," in *IEEE Transactions on Power Electronics*, vol. 21, no. 2, pp. 549-552, March 2006.

[23] F. Raab, "Radio Frequency Pulsewidth Modulation," in *IEEE Transactions on Communications*, vol. 21, no. 8, pp. 958-966, August 1973.

[24] H. Tebianian, J. Quaicoe and B. Jeyasurya, "High frequency full-bridge Class-D inverter using eGaN® FET with dynamic dead-time control," in *2016 IEEE PELS Workshop on Emerging Technologies: Wireless Power Transfer (WoW)*, 2016, pp. 95-99.

[25] Z. Ye, Y. Lei, Z. Liao and R. C. N. Pilawa-Podgurski, "Investigation of Capacitor Voltage Balancing in Practical Implementations of Flying Capacitor Multilevel Converters," in *IEEE Transactions on Power Electronics*, vol. 37, no. 3, pp. 2921-2935, March 2022.

[26] E. Solas, G. Abad, J. A. Barrena, S. Aurtenetxea, A. Carcar and L. Zajac, "Modular Multilevel Converter With Different Submodule Concepts—Part I: Capacitor Voltage Balancing Method," in *IEEE Transactions on Industrial Electronics*, vol. 60, no. 10, pp. 4525-4535, October 2013.

[27] F. F. Kuo, *Network Analysis and Synthesis*. New York: Wiley, 1962.

[28] I. V. Blagouchine and E. Moreau, "Analytic Method for the Computation of the Total Harmonic Distortion by the Cauchy Method of Residues," in *IEEE Transactions on Communications*, vol. 59, no. 9, pp. 2478-2491, September 2011.